

2 **Measuring directionality in double-beta decay and** 3 **neutrino interactions with kiloton-scale scintillation** 4 **detectors**

C. Aberle^a, A. Elagin^b, H.J. Frisch^b, M. Wetstein^b, and L. Winslow^{a*}

^a*University of California, Los Angeles, Los Angeles, CA 90095, USA*

^b*University of Chicago, Chicago, IL 60637, USA*

5 *E-mail: lwinslow@physics.ucla.edu*

ABSTRACT: Large liquid-scintillator-based detectors have proven to be exceptionally effective for low energy neutrino measurements due to their good energy resolution and scalability to large volumes. The addition of directional information using Cherenkov light and fast timing would enhance the scientific reach of these detectors, especially for searches for neutrino-less double-beta
6 decay. In this paper, we develop a technique for extracting particle direction using the difference in arrival times for Cherenkov and scintillation light, and evaluate several detector advances in timing, photodetector spectral response, and scintillator emission spectra that could be used to make direction reconstruction a reality in a kiloton-scale detector.

7 **KEYWORDS:** Scintillators, Large detector systems for particle and astroparticle physics; Neutrino
8 detectors; Simulation methods and programs.

*corresponding author

Contents

11	1. Introduction	1
12	2. Liquid scintillator detectors	2
13	3. Geant4 simulation	3
14	4. Detector timing	6
15	5. Detector wavelength response	7
16	6. Scintillator emission spectrum	7
17	7. Reconstruction	8
18	8. Energy dependence	10
19	9. Conclusions	11

1. Introduction

Liquid scintillator-based detectors are responsible for several of the critical measurements that have determined our present understanding of neutrino masses and mixings. These measurements include KamLAND's measurement of reactor anti-neutrino oscillation at a distance of ~ 200 km[1], Borexino's measurement of ^7Be solar neutrino oscillation[2], and most recently the short baseline reactor anti-neutrino experiments that measured oscillations due to θ_{13} at a distance of 1 km: Daya Bay[3], Double Chooz[4, 5], and RENO[6]. Scintillator-based neutrino detectors will continue to be important for the next set of neutrino measurements, from the determination of the neutrino mass hierarchy[7, 8] to elastic scattering measurements[9] and sterile neutrino searches[10, 11], and for non-proliferation applications[12, 13].

The scalability of these detectors to large volumes also makes them highly competitive for neutrino-less double-beta ($0\nu\beta\beta$) decay searches in which the final state consists of a pair of electrons with energies in the few MeV range. The observation of this rare decay would prove that the neutrino is a Majorana particle, which would have profound consequences to our understanding of the generation of mass and may provide a possible explanation of the matter-antimatter asymmetry in the universe. Currently one of the best limits for the $0\nu\beta\beta$ half-life comes from the scintillating detector KamLAND-Zen[14].

The advantage of liquid scintillators for measurements in the ~ 1 MeV range is their scalability from 1 ton to 1 kiloton while providing energy resolutions of $\sim 5\%$. This is roughly a factor of two

40 better than water Cherenkov detectors, the other developed technology that can be economically
41 scaled to these large masses. However, for scintillator-based detectors, while the energy resolution
42 is good due to the abundance of light, the light is isotropic and does not retain the directional infor-
43 mation of the primary particle. In contrast, the direction of the particle can be reconstructed from
44 the Cherenkov cone in water-based detectors, although the energy resolution rapidly degrades be-
45 low ~ 5 MeV. For double-beta decay in particular, but also for neutrino interactions, the directional
46 information can be a strong suppressant of backgrounds.

47 In a liquid-scintillation-based detector, Cherenkov light is also produced, although most is ab-
48 sorbed and re-emitted as part of the scintillation processes. However, some fraction retains its di-
49 rectional information. If this directional Cherenkov light can be isolated from the copious isotropic
50 scintillation light, it may be possible to reconstruct the direction of the primary particle or, in the
51 case of double-beta decay, to determine the existence and topology of the pair. The addition of di-
52 rectionality is thus a powerful tool for background rejection. In this paper, we develop a technique
53 for separating the Cherenkov and scintillation light using the photon arrival times and evaluate sev-
54 eral detector advances in timing, photodetector spectral response, and scintillator emission spectra
55 that would allow the realization of direction reconstruction in kilo-ton scale scintillating neutrino
56 detectors. This is a different technique and application than the direction reconstruction described
57 for high-energy neutrino interactions[15] or that for neutrons from inverse beta decay[16, 17].

58 2. Liquid scintillator detectors

59 Liquid scintillators are ‘cocktails’ of aromatic hydrocarbons. When charged particles move through
60 a scintillator, the molecules are excited, predominantly via the non-localized electrons in the π -
61 bonds of the phenyl groups[18]. Vibrational and rotational modes of the molecules are turned into
62 heat within picoseconds through collisions with other molecules. Within ~ 10 picoseconds, the
63 π -electrons de-excite to the first excited state from higher levels through radiationless transitions.
64 The first excited state can de-excite through photon emission. There are two characteristic times
65 for this de-excitation, depending if the singlet state or the triplet state was excited. The singlet state
66 will de-excite within nanoseconds while the triplet state de-excites on the order of 10’s or 100’s of
67 nanoseconds. These two processes are fluorescence and phosphorescence respectively. The exact
68 time constants for these processes are determined by the composition of the scintillator.

69 The absorption and emission spectra overlap at some level in all molecules. Consequently, if
70 there is only one type of molecule in the scintillator cocktail the light output is reduced due to inef-
71 ficiencies in the energy transfer through multiple absorption and re-emission processes. Aromatic
72 solutes or fluorophores are added to the primary solvent to shift the wavelengths of the photons
73 to higher values where the scintillator is more transparent. This wavelength-shifting is also used
74 to match the quantum efficiency as a function of wavelength for the photodetectors being used.
75 One typical scintillator mixture uses pseudocumene as the solvent with 1-5 g/l of PPO as the flu-
76 orophore. This mixture has a peak emission at about 400 nm where bialkali photomultiplier tubes
77 (PMTs) are most sensitive and the pseudocumene is relatively transparent.

A good liquid scintillator will produce $\sim 10,000$ photons isotropically per MeV of deposited
energy. Although less abundant, Cherenkov light will be produced as well if a particle is moving
faster than the speed of light in the medium. This light is emitted in a cone centered on the direction

of the particle trajectory, and with a continuous spectrum weighted toward shorter wavelengths but extending well into the red. The spectrum is described by[19]:

$$\frac{d^2N}{d\lambda dx} = \frac{2\pi\alpha Z^2}{\lambda^2} \left[1 - \frac{1}{\beta^2 n(\lambda)^2} \right] \quad (2.1)$$

where $n(\lambda)$ is the wavelength-dependent index of refraction and β is the velocity of the incoming particle. In a large detector, the Cherenkov light produced at wavelengths shorter than the absorption cutoff of the scintillator will be absorbed and re-emitted as isotropic light, but wavelengths longer than this cutoff will propagate across the detector, retaining their directional information. These undisturbed Cherenkov photons will have timing determined by the group velocity[20–22] in the liquid,

$$v_g(\lambda) = \frac{c_{vacuum}}{n(\lambda) - dn(\lambda)/d\log(\lambda)}. \quad (2.2)$$

78 The longer wavelength Cherenkov photons typically arrive before the scintillation light, which
79 is slowed by both the scintillation processes and the shorter wavelengths involved. Thus, with
80 sufficient timing resolution and sensitivity to longer wavelengths it should be possible to separate
81 the directional Cherenkov light and the isotropic scintillation light, and then to reconstruct the
82 direction of the initial particle.

83 In $0\nu\beta\beta$, the electrons emerge with a combined energy equal to the Q-value of the particular
84 isotope. The individual electrons follow distributions of energies and angular correlations, a proba-
85 ble case being equal division of energy between back-to-back electrons[23]. This case is shown in
86 figure 1 for an example ^{116}Cd $0\nu\beta\beta$ event. Since the decay half-life is inversely proportional to the
87 phase-space factor, isotopes with higher Q-values are preferred and due to backgrounds from the
88 daughters of the ^{238}U and ^{232}Th decay chains those with Q-values at or above 2.6 MeV are most
89 often considered for $0\nu\beta\beta$ searches. There are hundreds of candidate $0\nu\beta\beta$ isotopes[24], but only
90 a handful with large Q-values.

91 Most of the high Q-value candidates have been considered as a dopant for a liquid scin-
92 tillator: ^{150}Nd (Q=3.367 MeV)[25, 26], ^{96}Zr (Q=3.350 MeV)[27], ^{100}Mo (Q=3.034 MeV)[28],
93 ^{82}Se (Q=2.995 MeV)[29], ^{116}Cd (Q=2.81 MeV)[29, 30], ^{130}Te (Q=2.533 MeV)[29, 31], ^{136}Xe
94 (Q=2.479 MeV)[14] and ^{124}Sn (Q=2.29 MeV)[32]. Xenon gas readily dissolves into liquid scintil-
95 lator. For the other isotopes, a suitable organometallic compound needs to be found that produces a
96 stable scintillator with a long attenuation length in the wavelength region of interest. As an alterna-
97 tive to single-atom-doping, recently nanocrystals formed by candidate isotopes have been explored
98 as a dopant[29, 33].

99 3. Geant4 simulation

100 In order to study the effects relevant to directional reconstruction in liquid scintillators, a GEANT4
101 [34, 35] simulation has been constructed. The simulation uses GEANT4 version 4.9.6 with the
102 default liquid scintillator optical model, in which optical photons are assigned the group velocity
103 in the wavelength region of normal dispersion.

104 The detector geometry is a sphere of 6.5 m radius filled with scintillator. Figure 1 shows
105 the geometry and the Cherenkov light from an example ^{116}Cd $0\nu\beta\beta$ event. The default scintil-
106 lator properties have been chosen to match a KamLAND-like scintillator[36]: 80% n-dodecane,

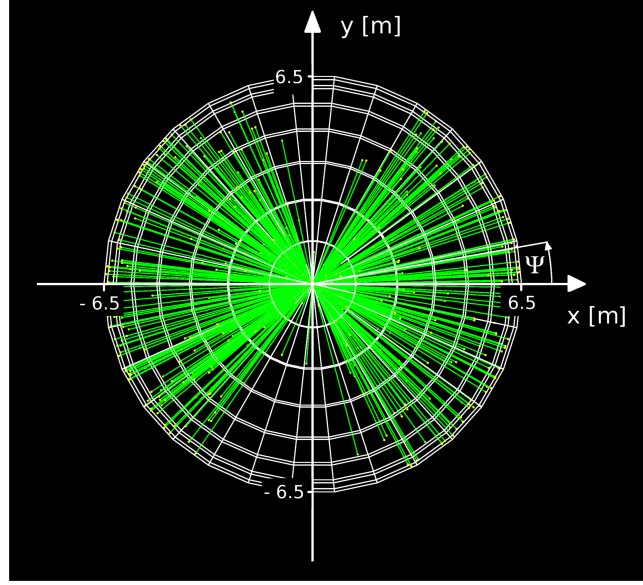


Figure 1. The detector geometry and coordinate system. The radial rays (green lines) are photons emitted by two back-to-back electrons with 1.4 MeV each (equally divided energy of ^{116}Cd $0\nu\beta\beta$ decay). The electrons originate at the center of the sphere with initial directions along the x and -x-axis. Only Cherenkov photons are drawn to illustrate the directionality of the event.

107 20% pseudocumene (1,2,4-trimethylbenzene) and 1.52 g/l PPO (2,5-diphenyloxazole). The scin-
 108 tillator properties implemented in the simulation include the atomic composition and density ($\rho =$
 109 0.78 g/ml), the wavelength-dependent attenuation length[37] and refractive index[38], the scintil-
 110 lation emission spectrum[37], emission rise time ($\tau_r = 1.0$ ns) and emission decay time constants
 111 ($\tau_{d1} = 6.9$ ns and $\tau_{d2} = 8.8$ ns with relative weights of 0.87 and 0.13)[39], scintillator light yield
 112 (9030 photons/MeV) and the Birks constant ($kB \approx 0.1$ mm/MeV)[40]. Variations from the base-
 113 line KamLAND case are discussed below. Re-emission of absorbed photons in the scintillator bulk
 114 volume and scattering have not yet been included, but are not expected to change the conclusions
 115 here.

116 The inner sphere surface is used as the photodetector. It is treated as fully absorbing (no reflec-
 117 tions), with a photodetector coverage of 100%. Two important photodetector properties have been
 118 varied: 1) the transit-time spread (TTS, default $\sigma = 0.1$ ns) and 2) the wavelength-dependent quan-
 119 tum efficiency (QE) for photoelectron production. The default is the QE of a bi-alkali photocathode
 120 (Hamamatsu R7081 PMT)[41], for which digitized values come from the Double Chooz[4] Monte
 121 Carlo simulation. We note that the KamLAND 17-inch PMTs use the same photocathode type with
 122 similar quantum efficiency.

123 The studies in sections 3 to 7 are made with single 5 MeV electrons, lower energies are dis-
 124 cussed in section 8. Future studies will work on increasing the complexity of the event as is needed
 125 for $0\nu\beta\beta$ studies. Three effects primarily contribute to the timing of the scintillator detector sys-
 126 tem. First, the simulated travel time of an initial 5 MeV electron is typically between 0.10 and
 127 0.15 ns, while the travel distance is about 3 cm. Second, the scintillation light emission follows a

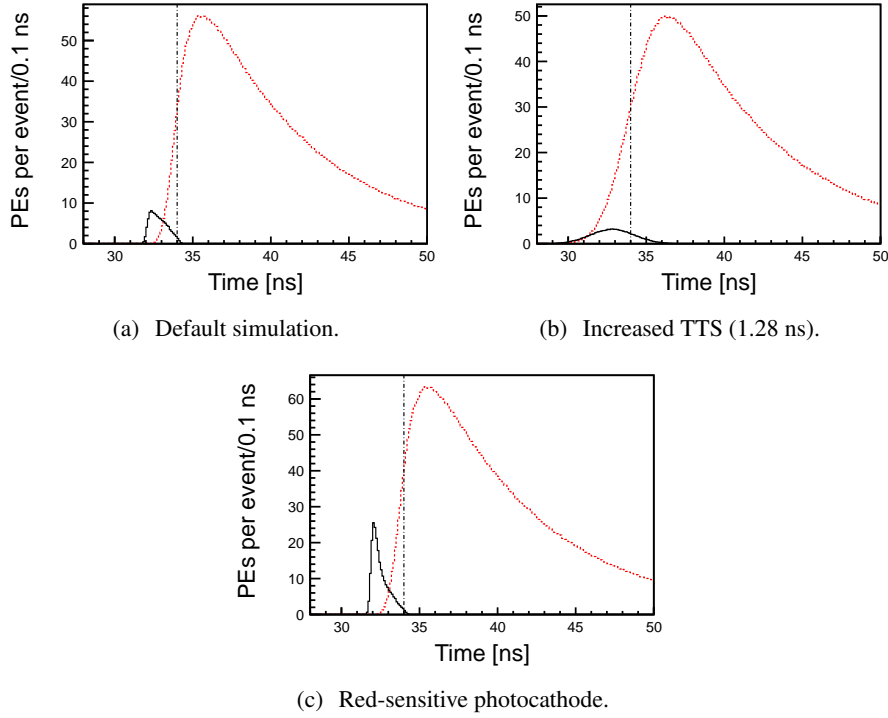


Figure 2. Photoelectron (PE) arrival times after application of the transit-time spread (TTS) for the simulation of 1000 electrons (5 MeV) with different values of the TTS and wavelength response. PEs from Cherenkov light (black, solid line) and scintillation light (red, dotted line) are compared. The dash-dotted vertical line illustrates a time cut at 34.0 ns. (a) Default simulation: bialkali photocathode and TTS = 0.1 ns (σ). After the 34.0 ns time cut we get 171 PEs from scintillation and 108 PEs from Cherenkov light. (b) Default simulation settings except for TTS = 1.28 ns (KamLAND 17 in. PMTs). After the 34.0 ns time cut we get 349 PEs from scintillation and 88 PEs from Cherenkov light. (c) Default simulation settings except for a GaAsP photocathode. After the 34.0 ns time cut we get 226 PEs from scintillation and 229 PEs from Cherenkov light.

128 distribution characterized by scintillator-specific rise and decay times. Before the solutes in liquid
 129 scintillator can emit optical photons, the energy has to be transferred from the solvent to the solute.
 130 The time constant of this energy transfer accounts for a rise time in scintillation light emission. Past
 131 neutrino experiments were not highly sensitive to the effect of the scintillation rise time, which is
 132 the reason why there is a lack of accurate numbers. We assume a rise time of 1.0 ns; more detailed
 133 studies are needed in the future. The two time constants used to describe the falling edge of the
 134 scintillator emission time distribution (quoted above) are values specific to the KamLAND scintil-
 135 lator. Third, chromatic dispersion turns out to be an important effect in a 6.5m-radius detector at
 136 the level of precision needed for direction reconstruction.

137 Due to the wavelength-dependence of the refractive index the speed of light in the scintillator
 138 (see Equation (2.2)) increases with increasing photon wavelengths for normal dispersion, with red
 139 light traveling faster than blue light. In order to study the measurability of the time differences, we
 140 simulated 5 MeV electrons at the center of the sphere where we used instantaneous scintillation

emission with the quantum-efficiency applied, but not including a transit-time spread. The true hit time distributions of photoelectrons were analyzed for scintillation light and Cherenkov light separately. Photoelectrons coming from Cherenkov light are on average created about 0.5 ns earlier than PEs from scintillation light. The RMS values from PE time distributions for Cherenkov and scintillation light are both about 0.5 ns. Note that these numbers include the effect of the finite electron travel time.

The measurement of the arrival times of single photoelectrons is affected by the transit-time spread (TTS) of the photodetectors, a number which can be different by orders of magnitude depending on the detector type. The default TTS of 0.1 ns (σ) is a value which can be achieved with the large area picosecond photodetectors (LAPPDs)[42, 43] and possibly hybrid photodetectors (HPDs)[44]; even significantly lower TTS numbers are realistic with the LAPPD[45–47]. We note that uncertainties in the vertex reconstruction will produce a similar effect to the smearing due to the TTS.

In Sections 4 to 6, we study the photoelectron timing for different detector configurations. We focus on the idea of increasing the discrimination between Cherenkov and scintillation light by using improved detector timing. The primary quantities provided by the GEANT4 simulation are the photoelectron hit positions and the detection times after the TTS resolution has been applied. In Section 7 these quantities are then used for event reconstruction.

4. Detector timing

We first discuss results for the default simulation settings described in the previous section. Figure 2 (a) shows the TTS-smeared photoelectron (PE) detection times for 1000 simulated electrons with 5 MeV energy in the center of the detector, with initial momentum directions coinciding with the x-axis. The photoelectrons induced by Cherenkov light arrive earlier, as expected due to the instantaneous emission and the higher average photon speed compared to scintillation light. There is, however, significant overlap of the two arrival time distributions.

In order to compare simulations with different parameters, a fixed time cut of $t \leq 34.0$ ns is applied using the truth information to isolate the Cherenkov light in this early time window. For the default simulation case, the average number of PEs per event coming from Cherenkov light in the early time window (108) is 98% of the total average number of PEs from Cherenkov light (110). For scintillation light, the average number of PEs (171) is only 3.1% of the average total scintillation-induced PEs (5445). This demonstrates the effectiveness of a time cut to separate Cherenkov light from scintillation light.

The ratio of Cherenkov-induced to scintillation-induced photoelectrons in the early time window ($R_{C/S}$) is a useful figure-of-merit when comparing different simulation settings, since a higher ratio means more directional information per PE. For the default simulation settings $R_{C/S} = 0.63$.

Figure 3 displays the angular distribution of PE hits after the time cut. Although this time cut is a simplification of actual time reconstruction effects, we can use it to indicate the spatial distribution of hits in the early time window. The Cherenkov ring structure can be clearly seen in the peak near 46° , demonstrating that the directional signal conveyed by the Cherenkov photons is not erased by scattering of the initial 5 MeV electrons.

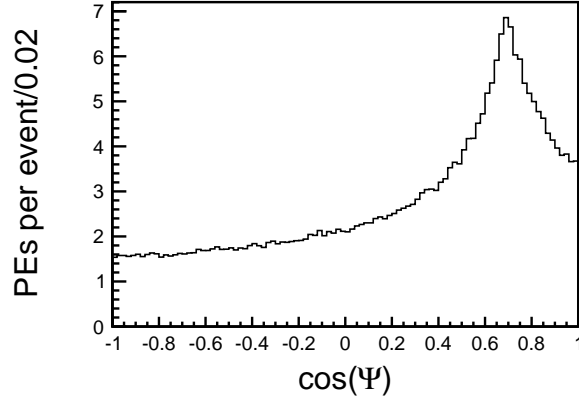


Figure 3. The angular distribution of photoelectron hits relative to the original electron direction, $\cos(\Psi) = x_{hit}/|\vec{r}_{hit}|$. The sample consists of 1000 events with a 5 MeV electron produced at the detector center. Default simulation settings are used and both Cherenkov and scintillation light are included. The $t \leq 34.0$ ns cut is applied.

181 When the 17-inch KamLAND PMTs[37, 48] (TTS = 1.28 ns) are used in the simulation, the
 182 broadening of the time distributions leads to a strongly decreased ratio of Cherenkov over scintilla-
 183 tion light ($R_{C/S} = 0.25$) for $t < 34.0$ ns (see figure 2 (b)). This shows that a low photodetector TTS
 184 is critical for directionality reconstruction and motivates the use of novel photodetector types.

185 5. Detector wavelength response

186 In addition to decreasing the photodetector TTS to enhance $R_{C/S}$, it is possible to optimize the
 187 wavelength-dependence of the photocathode. Since Cherenkov photons which pass through meters
 188 of scintillator have on average longer wavelengths than scintillation photons, a photodetector which
 189 is more sensitive at long wavelengths increases not only the absolute number of PEs but also the
 190 ratio between Cherenkov- and scintillation-induced PEs.

191 We have run the simulation with the QE of an extended red-sensitive GaAsP photocathode
 192 (Hamamatsu R3809U-63)[49]. Figure 2(c) shows the results for the modified simulation with
 193 high QE in the red spectral region. The higher absolute number of photoelectrons coming from
 194 Cherenkov light (factor of ≈ 2) and the increased Cherenkov/scintillation ratio ($R_{C/S} = 1.01$) in the
 195 early time window would significantly improve the directionality reconstruction.

196 6. Scintillator emission spectrum

197 An alternative route towards increasing the separation in time between Cherenkov and scintillation
 198 photon hits is the tuning of the scintillator emission spectrum. Recently, the use of quantum dots
 199 (QDs) in liquid scintillators has been studied as a possibility to improve future large scale neutrino
 200 experiments[29, 33]. One major motivation for quantum-dot-doped scintillator is control of the
 201 emission spectra by tuning the size or composition of the quantum dots; quantum dots can also
 202 provide a mechanism for introducing an isotope for studying double-beta decay.

The emission spectrum of commercial alloyed core/shell $\text{CdS}_x\text{Se}_{1-x}/\text{ZnS}$ quantum dots was measured in Ref.[33]. This spectrum shows a symmetric peak centered around 461 nm with FWHM = 29 nm. In order to isolate the effect of the different emission spectrum, the other simulation settings, including the KamLAND absorption spectrum, were kept unchanged; we find $R_{C/S} = 0.17$ for the default 34.0 ns timing cut. Compared to the default case shown in figure 2(a) the separation is worse (as expected) because the scintillation light wavelengths are longer than in the KamLAND emission spectrum.

However, advances in the production of commercial quantum dot samples could yield quantum dots which have similar, single peak emission shapes at lower wavelengths. This case has been simulated using the same spectral shape of the measured core-shell quantum dot emission but shifted to lower wavelengths such that the emission peak is centered at 384 nm. This peak emission value has been measured for other types of QDs, however with a much more pronounced tail[33]. The resulting PE time distribution shows improved separation of Cherenkov and scintillation light compared to the default simulation. After the 34.0 ns cut on the TTS-smeared PE time we obtain a Cherenkov/scintillation ratio of $R_{C/S} = 0.86$ (107 PE from Cherenkov light and 124 PE from scintillation). The number of Cherenkov-induced PEs after the time cut is unchanged while the number of PEs coming from scintillation light is decreased due to the higher average photon travel times.

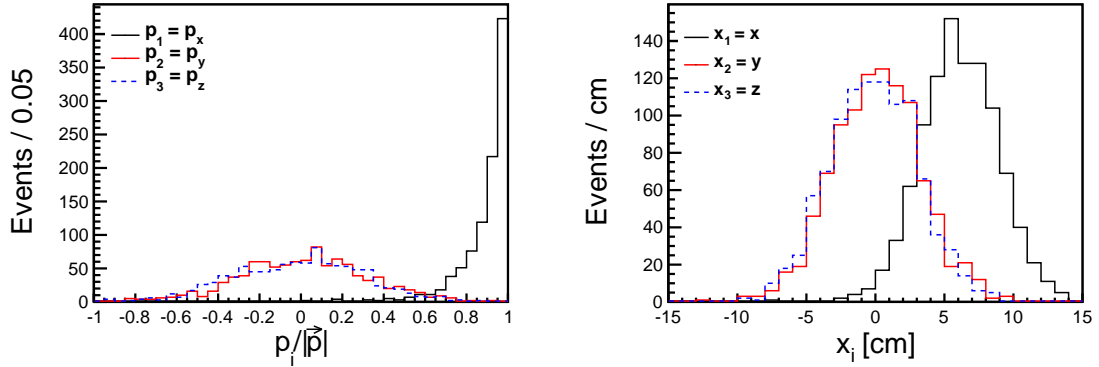


Figure 4. (Left) The reconstructed direction, $(p_x/|\vec{p}|, p_y/|\vec{p}|, p_z/|\vec{p}|)$, for the simulation of 1000 electrons (5 MeV). In the simulation the electrons are produced along the x-axis, $\vec{p}/|\vec{p}| = (1,0,0)$, and originate from the center of the 6.5m-radius detector, $\vec{r} = (0,0,0)$. Only photons with arrival time of $t < 34.0$ ns are used in the reconstruction. The quantum efficiency of the bialkali photocathode is taken into account. (Right) The reconstructed vertex position, (x,y,z) , for the same simulation.

7. Reconstruction

The timing studies show that in the early time window, $t \leq 34.0$ ns, the ratio $R_{C/S}$ is high, improving the photoelectron hit selection. In this section, we apply reconstruction tools for a water Cherenkov detector, WCSimAnalysis, to the problem of reconstructing the position and direction of 5 MeV electrons from this early light. WCSimAnalysis is a water Cherenkov reconstruction

package developed for the Long Baseline Neutrino Experiment (LBNE collaboration)[50]. It provides a framework for generic event cleaning, track reconstruction, and particle identification, and comes equipped with variety of pre-built algorithms. It is continuing to be expanded using new track-fitting techniques for water Cherenkov detectors[51] based on advanced photosensors with sub-cm imaging capabilities and timing resolutions below 100 picoseconds[42, 43].

The results presented in this paper rely on a simple vertex reconstruction algorithm, commonly known as a “point fit”[52]. It assumes that all of the scintillation and Cherenkov light is emitted from a single point in space-time (x_0, y_0, z_0, t_0) . In actuality, the light is emitted along an extended, multi-scattered electron track. However, at the energies discussed in this paper, the extent of this track is small (a few cm) compared to the scale of the detector ($R=6.5$ meters) and therefore the typical photon transit distances.

The first step of the reconstruction process relies on exact numerical calculations of vertex candidates from quadruplets of hits. Given a single point source, we need four constraints to solve for the four unknowns of the vertex (x, y, z, t_0) [53]. This approach would provide an exact solution in the case of four prompt, un-scattered photons originating from a common point. However, many of these randomly chosen quadruplets will produce anomalous solutions due to ‘real world’ effects such as delayed emission and deviations from the point-like geometry. Nonetheless, we found that any chosen subset of 400 quadruplets was a sufficiently large ensemble to assure that some solutions will be close to the true vertex.

Once a set of vertex candidates has been found, we test the goodness of each vertex and select the one that best fits the full ensemble of photon hits. The goodness of fit is determined based on the distribution of an observable known as the “point time residual”[52]. The point time residual is calculated by taking the difference between the measured time of a photon hit, and the predicted time of the hit, given its distance from the vertex hypothesis, a single effective speed of light in the scintillator, and the hypothesized t_0 of the event. The width of the time residual distribution over all hits is minimized when the hypothesized vertex is near the true vertex. Based on this figure of merit, we select the vertex with the narrowest time residual distribution from among the 400 candidates.

The direction of the electron track is then determined by taking the centroid of all vectors pointing from the fitted vertex to the hits on the detector. Since the Cherenkov light is highly directional, and since the timing cut enhances the purity of the Cherenkov light in the sample, this calculation provides a good measure of the track direction.

For the purpose of testing the reconstruction algorithm we use 1000 simulated electrons with an energy of 5 MeV, lower energies are studied in the next section. The electrons are simulated at the center of the detector, $\vec{r} = (0,0,0)$, along the x-axis, $\vec{p}/|\vec{p}| = (1,0,0)$. Figure 4 shows the vertex reconstruction. The vertex is reasonably well reconstructed around the center of the detector, $\vec{r} = (0,0,0)$, except along the x-axis. The RMS values of the distributions for all three reconstructed coordinates are smaller than 3.5 cm. The shift along the x-axis is due to two effects for which the reconstruction has to use average values rather than the unknown true value for each hit: the wavelength and hence the speed of the light in the medium, and the point of emission for each of the photons, reconstructed as coming from a common point. The reconstruction of the direction also is shown in figure 4. It shows that for the majority of the events the initial electron direction is reconstructed well. This is a promising result given the simplicity of the algorithms used.

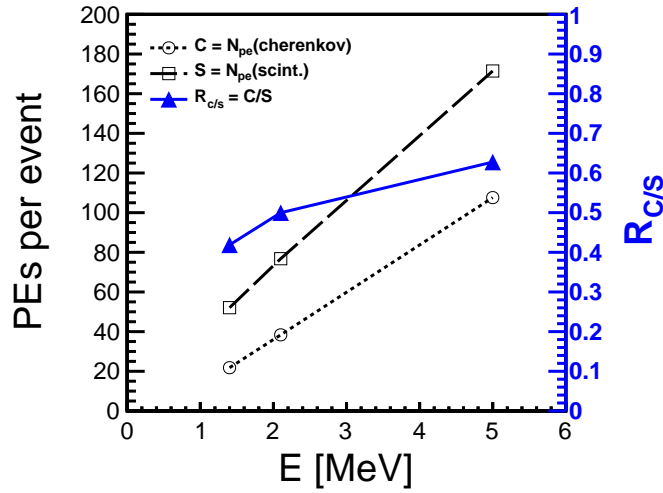


Figure 5. The energy dependence of the mean number of PEs after the 34.0 ns time cut is shown for Cherenkov-induced PEs (black open circles, dotted line) and scintillation-induced PEs (black open squares, dashed line). The ratio between the mean number of Cherenkov-induced and scintillation-induced PEs is shown as blue filled triangles, values are given on the right y-axis. The statistical errors are too small to be seen.

8. Energy dependence

In the previous sections we presented results on single 5 MeV electrons. In this section we study two lower energies, 1.4 MeV and 2.1 MeV. These energies correspond to $Q/2$ for the double-beta decay of ^{116}Cd and ^{48}Ca , respectively[31]. The isotope ^{116}Cd was chosen because of its potential use in quantum-dot-doped scintillators[29, 33] and ^{48}Ca was chosen to cover the Q -value range of $0\nu\beta\beta$ candidate isotopes.

The two additional simulation sets with 1.4 MeV and 2.1 MeV electrons were generated using the default simulation configuration described in section 3. The PE time distribution for the default settings is shown in figure 2 (a) for 5 MeV electrons. The shape of the scintillation and Cherenkov spectra is similar for the lower energies (not shown here). In figure 5, the energy-dependent mean number of PEs per event after the 34.0 ns time cut is shown for Cherenkov-induced and scintillation-induced PEs, as well as their ratio $R_{C/S}$. The mean number of PEs from Cherenkov (scintillation) light is 21.8 (52.1), 38.4 (76.8) and 108 (171) for 1.4 MeV, 2.1 MeV and 5 MeV, respectively. This gives the ratios $R_{C/S} = 0.42, 0.50$ and 0.63 : The decrease in Cherenkov-induced PEs is stronger than the decrease in scintillation-induced PEs as the energy is lowered.

The reconstruction algorithms outlined in section 7 have also been applied to the simulations at lower energies. Figure 6 shows the results for the lowest simulated electron energy, 1.4 MeV. Most events are still reconstructed well, despite the lower number of PEs and the decreased $R_{C/S}$. For 1.4 MeV electrons, the distribution RMS values for all three reconstructed coordinates are smaller than 4.5 cm. The mean cosine of the angle between the true direction and the reconstructed direction for different energies of the initial electron is shown in figure 7. The direction reconstruction performance is still promising for energies as low as 1.4 MeV.

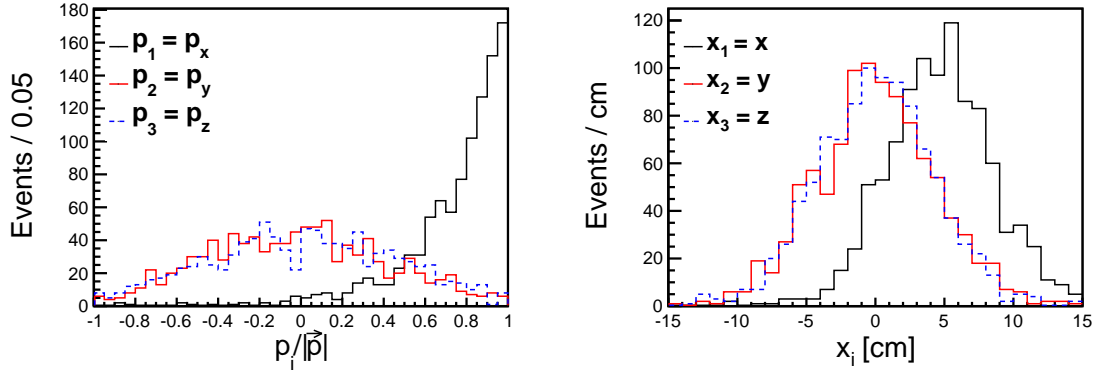


Figure 6. (Left) The reconstructed direction, $(p_x/|\vec{p}|, p_y/|\vec{p}|, p_z/|\vec{p}|)$, for the simulation of 1000 electrons (1.4 MeV). In the simulation the electrons are produced along the x-axis, $\vec{p}/|\vec{p}| = (1,0,0)$, and originate from the center of the 6.5m-radius detector, $\vec{r} = (0,0,0)$. Only photons with arrival time of $t < 34.0$ ns are used in the reconstruction. The quantum efficiency of the bialkali photocathode is taken into account. (Right) The reconstructed vertex position, (x,y,z) , for the same simulation.

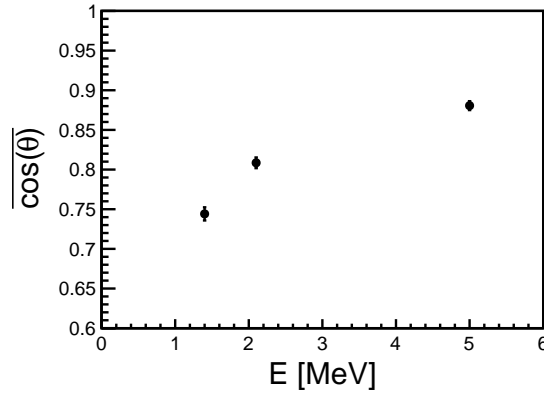


Figure 7. Mean cosine of the angle between the true initial electron direction and the reconstructed direction, as a function of the electron energy. For each energy 1000 events have been simulated. Statistical errors are shown.

291 9. Conclusions

292 The ability to reconstruct direction in kiloton-scale scintillation detectors would be a major techno-
 293 logical advance for neutrino experiments, especially those also searching for neutrino-less double-
 294 beta decay. More generally, this technique could be applied wherever scintillation-based detectors
 295 are used. A GEANT4 simulation of a simple spherical detector corresponding to a kiloton of scin-
 296 tillator shows that timing on the order of 0.1 ns is required to separate the directional Cherenkov
 297 light from the more abundant scintillation light. The separation can be improved using photode-
 298 tectors with more red sensitivity and liquid scintillators with a more narrow emission spectrum
 299 shifted to shorter wavelengths. Furthermore, simple reconstruction algorithms adapted from those
 300 for water Cherenkov detectors are able to reliably reconstruct the position and direction of elec-

trons with energies in the few MeV range. More detailed simulation and advanced reconstruction algorithms will need to be developed to move to more complicated event topography, such as those in neutrino-less double-beta decay, but the technique already appears promising.

Acknowledgments

The authors thank Andrew Blake at University of Cambridge for his work authoring the WCSimAnalysis code. The authors thank the neutrino reconstruction group at Iowa State, particularly Mayly Sanchez, Ioana Anghel, and Tian Xin, for their continued work in developing the WCSimAnalysis algorithms and for their insights and expertise regarding issues related to Cherenkov reconstruction with fast-timing. The authors also thank Michael Smy for his development of the quadruplet-based vertex-finding method. L. Winslow would like to thank Janet Conrad for many useful discussion on the topic, and Katsushi Arisaka for discussions on the possible reach of traditional PMTs and the characteristics of HPDs. C. Aberle and L. Winslow are supported by funds from University of California Los Angeles. The work at the University of Chicago is partially supported by DOE contract DE-SC0008172 and NSF grant PHY-1066014. Matthew Wetstein gratefully acknowledges support by the Grainger Foundation.

References

- [1] KamLAND collaboration, A. Gando et al., *Reactor On-Off Antineutrino Measurement with KamLAND*, arXiv:1303.4667.
- [2] Borexino collaboration, G. Bellini et al., *Precision measurement of the ^7Be solar neutrino interaction rate in Borexino*, *Phys. Rev. Lett.* **107** (2011) 141302, [arXiv:1104.1816].
- [3] Daya Bay collaboration, F. An et al., *Improved Measurement of Electron Antineutrino Disappearance at Daya Bay*, *Chin. Phys.* **C37** (2013) 011001, [arXiv:1210.6327].
- [4] Double Chooz collaboration, Y. Abe et al., *Reactor electron antineutrino disappearance in the Double Chooz experiment*, *Phys. Rev.* **D86** (2012) 052008, [arXiv:1207.6632].
- [5] Double Chooz collaboration, Y. Abe et al., *First Measurement of θ_{13} from Delayed Neutron Capture on Hydrogen in the Double Chooz Experiment*, *Phys. Lett.* **B723** (2013) 66, [arXiv:1301.2948].
- [6] RENO collaboration, J. K. Ahn et al., *Observation of Reactor Electron Antineutrinos Disappearance in the RENO Experiment*, *Phys. Rev. Lett.* **108** (2012) 191802.
- [7] Y.-F. Li, J. Cao, Y. Wang, and L. Zhan, *Unambiguous Determination of the Neutrino Mass Hierarchy Using Reactor Neutrinos*, arXiv:1303.6733.
- [8] *RENO-50 - International Workshop on toward Neutrino Mass Hierarchy*, June, 2009.
- [9] J. Conrad, M. Shaevitz, I. Shimizu, J. Spitz, M. Toups, and L. Winslow, *Precision $\bar{\nu}_e$ -electron Scattering Measurements with IsoDAR to Search for New Physics*, arXiv:1307.5081. In preparation, for submission to *Phys. Rev. D*.
- [10] IsoDAR collaboration, A. Bungau et al., *Proposal for an Electron Antineutrino Disappearance Search Using High-Rate ^8Li Production and Decay*, *Phys. Rev. Lett.* **109** (2012) 141802, [arXiv:1205.4419].
- [11] K. Heeger, B. Littlejohn, and H. Mumm, *Multiple Detectors for a Short-Baseline Neutrino Oscillation Search Near Reactors*, arXiv:1307.2859.
- [12] A. Porta et al., *Reactor Neutrino Detection for Non-Proliferation With the NUCIFER Experiment*, *Nuclear Science, IEEE Transactions on* **57** (2010) 2732–2739.
- [13] N. Bowden et al., *Experimental results from an antineutrino detector for cooperative monitoring of nuclear reactors*, *Nucl. Instrum. Meth.* **A572** (2007) 985 – 998.
- [14] KamLAND-Zen collaboration, A. Gando et al., *Limit on Neutrinoless $\beta\beta$ Decay of Xe-136 from the First Phase of KamLAND-Zen and Comparison with the Positive Claim in Ge-76*, *Phys. Rev. Lett.* **110** (2013) 062502, [arXiv:1211.3863].
- [15] J. G. Learned, *High Energy Neutrino Physics with Liquid Scintillation Detectors*, arXiv:0902.4009.
- [16] CHOOZ collaboration, M. Apollonio et al., *Search for neutrino oscillations on a long baseline at the CHOOZ nuclear power station*, *Eur.Phys.J.* **C27** (2003) 331–374, [hep-ex/0301017].
- [17] K. A. Hochmuth, M. Lindner, and G. G. Raffelt, *Exploiting the directional sensitivity of the Double Chooz near detector*, *Phys.Rev.* **D76** (2007) 073001, [arXiv:0704.3000].
- [18] J.B. Birks, *The Theory and Practice of Scintillation Counting*. Pergamon Press, 1964.
- [19] P. A. Cherenkov, *Visible emission of clean liquids by action of gamma radiation*, *Doklady Akademii Nauk SSSR* **2** (1934) 451.

- [20] A. M. Steinberg, P. G. Kwiat, and R. Y. Chiao, *Dispersion cancellation in a measurement of the single-photon propagation velocity in glass*, *Phys. Rev. Lett.* **68** (1992) 2421–2424.
- [21] Particle Data Group, J. Beringer et al., *Review of Particle Physics (RPP)*, *Phys. Rev.* **D86** (2012) 010001.
- [22] I. Tamm, *Radiation Emitted by Uniformly Moving Electrons*, *J. Phys. U.S.S.R.* **1** (1939) 439.
- [23] J. Kotila and F. Iachello, *Phase-space factors for double- β decay*, *Phys. Rev. C* **85** (2012) 034316.
- [24] V. Tretyak and Y. Zdesenko, *Tables of double beta decay data*, *Atomic Data and Nuclear Data Tables* **61** (1995) 43 – 90.
- [25] M. Yeh, Y. Williamson, and R. L. Hahn, *Metal-loaded liquid scintillators for neutrino experiments*, *J. Phys. Conf. Ser.* **136** (2008) 042054.
- [26] I. Barabanov et al., *A Nd-loaded liquid organic scintillator for the experiment aimed at measuring double beta decay*, *Instrum. Exp. Tech.* **55** (2012) 545–550.
- [27] Y. Fukuda, S. Moriyama, and I. Ogawa, *Development of liquid scintillator containing a zirconium complex for neutrinoless double beta decay experiment*, article in press, *Nucl. Instrum. Meth. A*, 2013.
- [28] V. Gehman, P. Doe, R. Robertson, D. Will, H. Ejiri, and R. Hazama, *Solubility, Light Output and Energy Resolution Studies of Molybdenum-Loaded Liquid Scintillators*, *Nucl. Instrum. Meth.* **A622** (2010) 602–607, [[arXiv:0911.2198](#)].
- [29] L. Winslow and R. Simpson, *Characterizing quantum-dot-doped liquid scintillator for applications to neutrino detectors*, *Journal of Instrumentation* **7** (2012) P07010.
- [30] G. Bellini et al., *High sensitivity 2 beta decay study of Cd-116 and Mo-100 with the BOREXINO counting test facility (CAMEO project)*, *Eur. Phys. J.* **C19** (2001) 43–55, [[nucl-ex/0007012](#)].
- [31] S. D. Biller, *Probing Majorana neutrinos in the regime of the normal mass hierarchy*, *Phys. Rev.* **D87** (2013) 071301, [[arXiv:1306.5654](#)].
- [32] KIMS collaboration, M. Hwang et al., *Development of tin-loaded liquid scintillator for the double beta decay experiment*, *Nucl. Instrum. Meth.* **A570** (2007) 454–458.
- [33] C. Aberle, J. Li, S. Weiss, and L. Winslow, *Optical properties of quantum-dot-doped liquid scintillators*, *Journal of Instrumentation* **8** (2013) P10015, [[arXiv:1307.4742](#)].
- [34] GEANT4 collaboration, S. Agostinelli et al., *GEANT4: A Simulation toolkit*, *Nucl. Instrum. Meth.* **A506** (2003) 250–303.
- [35] J. Allison et al., *Geant4 developments and applications*, *Nuclear Science, IEEE Transactions on* **53** (2006) 270–278.
- [36] KamLAND collaboration, K. Eguchi et al., *First results from KamLAND: Evidence for reactor anti-neutrino disappearance*, *Phys. Rev. Lett.* **90** (2003) 021802, [[hep-ex/0212021](#)].
- [37] O. Tajima, *Development of Liquid Scintillator for a Large Size Neutrino Detector*, Master’s thesis, Tohoku University, 2000.
- [38] O. Perevozchikov, *Search for electron antineutrinos from the sun with KamLAND detector*. PhD thesis, University of Tennessee, 2009.
- [39] O. Tajima, *Measurement of Electron Anti-Neutrino Oscillation Parameters with a Large Volume Liquid Scintillator Detector, KamLAND*. PhD thesis, Tohoku University, 2003.

- [40] C. Grant, *A Monte Carlo Approach to ^7Be Solar Neutrino Analysis with KamLAND*. PhD thesis, University of Alabama, 2012.
- [41] Hamamatsu Photonics K.K., *Large Photocathode Area Photomultiplier Tubes (data sheet, including R7081)*, accessed July, 2013. http://www.hamamatsu.com/resources/pdf/etd/LARGE_AREA_PMT_TPMH1286E05.pdf.
- [42] J. Anderson et al., *The Development of Large-Area Fast Photo-detectors*, 2009. <http://psec.uchicago.edu/library/doclib/documents/60/>.
- [43] LAPPD collaboration, *Technical Design Report for the frugal MCP*, 2010. http://psec.uchicago.edu/library/doe_reports/TDR.pdf.
- [44] Y. Kawai, *Development of a Hybrid Photon-Detector Module for Next Generation Water-Cherenkov Detectors*. PhD thesis, The Graduate University for Advanced Studies (SOKENDAI), 2007.
- [45] B. Adams et al., *Invited article: A test-facility for large-area microchannel plate detector assemblies using a pulsed sub-picosecond laser*, *Review of Scientific Instruments* **84** (2013) 061301.
- [46] E. Oberla, J. Genat, H. Grabas, H. Frisch, K. Nishimura, and G. Varner, *A 15 GSa/s, 1.5 GHz Bandwidth Waveform Digitizing ASIC*, submitted to Nucl. Instrum. Meth. A, 2013.
- [47] H. Grabas et al., *RF strip-line anodes for Psec large-area MCP-based photodetectors*, *Nucl. Instrum. Meth. A* **711** (2013) 124 – 131.
- [48] H. Kume et al., *20 INCH DIAMETER PHOTOMULTIPLIER*, *Nucl. Instrum. Meth.* **205** (1983) 443–449.
- [49] Hamamatsu Photonics K.K., *R3809U-61/-63/-64 data sheet*, accessed July, 2013. http://www.hamamatsu.com/resources/pdf/etd/R3809U-61-63-64_TPMH1295E04.pdf.
- [50] A. Blake, *WCSimAnalysis Reconstruction Package*. Cavendish Laboratory, University of Cambridge, UK.
- [51] M. Sanchez and M. Wetstein, *Using Large Area Microchannel Plate Photodetectors in the Next Generation Water Cherenkov Neutrino Detectors*, *Nuclear Physics B - Proceedings Supplements* **229232** (2012) 525. Neutrino 2010.
- [52] M. Ishitsuka, *L/E Analysis of the Atmospheric Neutrino Data From Super-Kamiokande*. PhD thesis, University of Tokyo, 2004.
- [53] M. Smy for the Super-Kamiokande collaboration, *Low Energy Event Reconstruction and Selection in Super-Kamiokande-III*, in *Proceedings of the 30th International Cosmic Ray Conference* (R. Caballero, J.C. D’Olivo, G. Medina-Tanco, L. Nellen, F.A. Sánchez, J.F. Valdés-Galicia, ed.), vol. 5, pp. 1279–1282, 2008.